Electromagnetic wave propagation in anisotropic metamaterials created by a set of periodic inductor-capacitor circuit networks

Yijun Feng,* Xiaohua Teng, Yan Chen, and Tian Jiang
Department of Electronic Science and Engineering, State Key Lab of Modern Acoustics, Nanjing University, Nanjing, 210093, People's Republic of China
(Received 8 July 2005; revised manuscript received 3 October 2005; published 9 December 2005)

We propose a complete set of periodic circuit networks which can realize electromagnetic wave propagation in different two-dimensional (2D) isotropic and anisotropic metamaterials (AMMs). We synthesize the periodic circuits with unit cells of series capacitor or inductor in orthogonal directions, together with either capacitor or inductor shunted to ground. The dispersion relations of the periodic circuits are derived by applying Bloch boundary conditions to the unit cell, which show either elliptic or hyperbolic dispersion surface in phase space. The effective constitutive parameters are obtained by choosing different types and values of the impedance elements in the unit cell. The validity of the circuit models is proved by showing examples that the anisotropic *L-C* circuits could exhibit the wave propagation characteristics of two 2D AMMs with different cutoff properties, called *never-cutoff* or *anti-cutoff* medium. We construct interfaces between isotropic normal medium and AMMs with properly designed *L-C* circuits and analyze the electromagnetic wave propagation using microwave circuit simulations. We demonstrate extraordinary electromagnetic wave reflection and refraction phenomena including negative refraction, total reflection with reversion of the critical angle and anomalous Brewster effect that have good agreements with the theoretical analysis. Furthermore, we show that the *L-C* circuit models of AMMs could lead to different approach of actual implementation of 2D AMMs through capacitance loaded transmission line metamaterials. The simulation on actual microstrip line structure demonstrates similar wave propagation phenomena of AMMs, and the losses in the structure only affect the magnitude of the propagating energy.

DOI: 10.1103/PhysRevB.72.245107 PACS number(s): 78.20.Ci, 41.20.Jb, 78.67.−n, 84.40.Dc

I. INTRODUCTION

Artificial electromagnetic metamaterials have significantly broadened the range of electromagnetic wave propagation phenomena available. In recent years, both theoretical and experimental works on isotropic metamaterials with simultaneously negative permittivity and permeability have indicated extraordinary phenomena of negative refraction and super lens with subwavelength focusing of electromagnetic wave.[1–13] Such artificial metamaterial, named as left-handed material (LHM) or double negative material (DNG), could be realized through two-dimensional (2D) isotropic structures either with periodic array of split-ring resonators (SRR) and conducting wires[3–6] or with periodic inductor-capacitor (*L-C*) loaded transmission lines (TL) circuit.[7–13] These structures have been successfully used to experimentally demonstrate backward-wave radiation, negative refraction and subwavelength focusing in the isotropic metamaterials at microwave frequencies.[12–15]

Anisotropic metamaterials (AMMs) for which some elements of the permittivity and permeability tensors have negative value have also been studied theoretically, which demonstrate anomalous electromagnetic wave refraction and reflection that occurs at the interface between normal medium and the anisotropic medium. Negative refraction could be realized in such media under some different combinations of its medium parameters.[16–18] The anisotropic media has been identified into four classes based on their electromagnetic wave propagation properties, which are called *cutoff*, *always-cutoff*, *never-cutoff* and *anti-cutoff* media.[17] More recently, experiment and simulation have confirmed the negative refraction in such AMM. *S*-polarized electromagnetic waves from a nearby source redirect to a partial focus inside a planar structure of AMM composed of split ring resonators, designed to provide a permeability equal to −1 along the longitudinal axis.[19]

However, since resonant structures such as SRRs are lossy and narrow-banded, they are often difficult to implement from a practical point of view. The TL circuit approach of metamaterials leads to non-resonant structures with lower loss and wider bandwidth. In this paper, we propose a complete set of periodic *L-C* circuit that could be used to realize the electromagnetic wave propagation in 2D AMMs. We synthesize the periodic circuits with unit cell of series capacitor and inductor in orthogonal directions, together with either capacitor or inductor shunted to ground. The dispersion relation of the anisotropic circuits derived by applying Bloch boundary conditions to the unit cell shows hyperbolic dispersion surface in phase space, therefore the anisotropic *L-C* circuits could exhibit the propagation characteristics of either 2D *never-cutoff* or *anti-cutoff* medium over certain operation frequency bandwidth. We have verified the *L-C* circuit models by constructing interfaces of normal media and AMMs with properly designed isotropic and anisotropic *L-C* circuits of finite size and analyzing the electromagnetic wave propagation through the interface using microwave circuit simulations tool of Agilent's Advanced Design System (ADS). We have demonstrated anomalous electromagnetic wave reflection and refraction phenomena that have good agreement with the theoretical analysis. Finally, we show that the *L-C*

circuit models of AMMs could lead to different approach of actual implementation of 2D AMMs. The simulation on example of capacitance loaded microstrip line structure demonstrates the wave propagation phenomenon of AMM.

II. ELECTROMAGNETIC WAVE PROPAGATION IN HOMOGENEOUS ANISOTROPIC METAMATERIALS

Consider a linear homogenous material characterized by relative permittivity and permeability tensors with only nonzero diagonal elements, having the following forms,

$$\varepsilon_r = \begin{pmatrix} \varepsilon_{xr} & 0 & 0 \\ 0 & \varepsilon_{yr} & 0 \\ 0 & 0 & \varepsilon_{zr} \end{pmatrix}, \quad \mu_r = \begin{pmatrix} \mu_{xr} & 0 & 0 \\ 0 & \mu_{yr} & 0 \\ 0 & 0 & \mu_{zr} \end{pmatrix}. \tag{1}$$

We assume a plane wave with the electric field polarized along the y axis having the following specific form similar to the discussion in Ref. 17

$$\mathbf{E} = \mathbf{e}_y e^{i(k_x x + k_z z - \omega t)}, \tag{2}$$

where the $\mathbf{e}_y$ is the unit vector along y axis, and k_x, k_z are the x and z components of the wave vector, respectively. The plane wave solutions specified by Eq. (2) satisfy the dispersion relation

$$\frac{k_z^2}{\varepsilon_{yr}\mu_{xr}\left(\frac{\omega}{c}\right)^2} + \frac{k_x^2}{\varepsilon_{yr}\mu_{zr}\left(\frac{\omega}{c}\right)^2} = 1. \tag{3}$$

In the absence of losses, the property of the plane wave solution in the anisotropic media is distinguished by the sign of k_z^2, which can be either a propagating wave or an evanescent wave. Considering both the positive and the negative value of ε_y, μ_x, and μ_z, Smith *et al.* have identified four classes of media based on their cutoff properties, which are called *cutoff*, *always-cutoff*, *never-cutoff* and *anti-cutoff* media.[17] Anomalous reflection and refraction phenomena including negative refraction have been revealed at the interface between vacuum and *never-cutoff* or *anti-cutoff* media, which has a dispersion relation of hyperbolic isofrequency surface. These phenomena are different from those occur at the interface between vacuum and the isotropic left-handed metamaterial. More recently, experiment and simulation have confirmed the negative refraction in such AMM composed of split ring resonators, designed to provide a permeability equal to -1 along the longitudinal axis.[19] In the following sections we propose another approach to realize the *never-cutoff* or *anti-cutoff* media by anisotropic *L-C* circuit networks.

III. ELECTROMAGNETIC WAVE PROPAGATION IN PERIODIC *L-C* NETWORKS

For conventional homogenous materials (sometimes named as right-handed materials, or RHMs), the dielectric properties like permittivity and permeability can be modeled by using distributed periodic *L-C* networks. The per-unit-length capacitance C and inductance L in the *L-C* networks

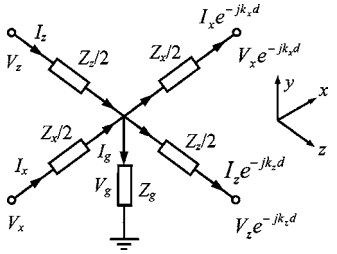

FIG. 1. The unit cell of a 2D anisotropic *L-C* circuit structure.

represent a positive equivalent permittivity and permeability, respectively. Recently, isotropic LHM has been successfully realized through the dual *L-C* configuration, in which the positions of C and L are simply interchanged, resulting equivalent material parameters of simultaneously negative values.[7–10] This periodic dual *L-C* network realized by *L-C* loaded TL circuit has been used to demonstrate negative refraction and focusing in LHM experimentally.[12,13]

To model the AMMs, we propose a set of periodic *L-C* circuit that could be used to realize the electromagnetic wave propagation in 2D AMMs. The electric and magnetic field components propagating in the AMMs could be appropriately mapped to the voltages and currents in the corresponding *L-C* networks.

Consider a general case of the 2D anisotropic *L-C* periodic network with the unit cell schematically shown in Fig. 1. For simplicity, we neglect losses in the network and all the impedance elements (Z_x, Z_z, and Z_g) could be either capacitance or inductance. Such periodic network could be analyzed by applying Kirchhoff's voltage and current laws to the unit cell in conjunction with the Bloch-Floquet periodic boundary conditions,[7] and yields the following set of linear equations:

$$V_x = \frac{1}{2}Z_x I_x + Z_g I_g,$$

$$V_z = \frac{1}{2}Z_z I_z + Z_g I_g,$$

$$Z_g I_g = \frac{1}{2}Z_x I_x e^{-jk_x d} + V_x e^{-jk_x d},$$

$$Z_g I_g = \frac{1}{2}Z_z I_z e^{-jk_z d} + V_z e^{-jk_z d},$$

$$I_x + I_z = I_x e^{-jk_x d} + I_z e^{-jk_z d} + I_g, \tag{4}$$

where d is the period of the unit cell, and k_x, k_z are the wave number in the x and z direction, respectively. Substituting the first two and the last equations into the third and fourth equations, yields the following simplified linear equations for I_x and I_z

TABLE I. Eight types of *L-C* networks that represent different anisotropic metamaterials.

L-C circuit unit cell			Corresponding homogenous media characteristics	
Z_x	Z_z	Z_g	Constitutive parameters	Media type
inductive	inductive	capacitive	$\varepsilon_y\mu_x>0,\ \varepsilon_y\mu_z>0$	*cutoff*
capacitive	capacitive	inductive		
capacitive	capacitive	capacitive	$\varepsilon_y\mu_x<0,\ \varepsilon_y\mu_z<0$	*always-cutoff*
inductive	inductive	inductive		
capacitive	inductive	capacitive	$\varepsilon_y\mu_x>0,\ \varepsilon_y\mu_z<0$	*never-cutoff*
inductive	capacitive	inductive		
inductive	capacitive	capacitive	$\varepsilon_y\mu_x<0,\ \varepsilon_y\mu_z>0$	*anti-cutoff*
capacitive	inductive	inductive		

$$\begin{bmatrix} Z_g(1-e^{-jk_xd})^2 - Z_xe^{-jk_xd} & Z_g(1-e^{-jk_zd})(1-e^{-jk_xd}) \\ Z_g(1-e^{-jk_xd})(1-e^{-jk_zd}) & Z_g(1-e^{-jk_zd})^2 - Z_ze^{-jk_zd} \end{bmatrix} \begin{bmatrix} I_x \\ I_z \end{bmatrix} = 0. \tag{5}$$

For nontrivial solutions, the determinant of the coefficient matrix of (5) must vanish, which yields the following dispersion equation for the periodic network:

$$Z_gZ_z\cos k_xd + Z_gZ_x\cos k_zd = \frac{1}{2}Z_xZ_z + Z_gZ_z + Z_gZ_x. \tag{6}$$

If the period of the unit cell is much less than the wave length, therefore, the per-unit-cell phase delays are small ($k_xd \ll 1$, $k_zd \ll 1$, the continuous medium approximation). Under these two conditions, the dispersion equation (6) simplifies to

$$\frac{(k_xd)^2}{-\frac{Z_x}{Z_g}} + \frac{(k_zd)^2}{-\frac{Z_z}{Z_g}} = 1. \tag{7}$$

This dispersion equation is similar to Eq. (3), therefore the voltage and current propagation in the anisotropic periodic *L-C* network is equivalent to the electromagnetic wave propagation in homogenous 2D AMMs. The equivalent permittivity ε_{ye}, permeability μ_{xe}, and μ_{ze} of the *L-C* network can be obtained by mapping between the two dispersion equations (7) and (3) as

$$\varepsilon_{ye}\mu_{xe} = -\left(\frac{1}{\omega d}\right)^2\frac{Z_z}{Z_g}, \quad \varepsilon_{ye}\mu_{ze} = -\left(\frac{1}{\omega d}\right)^2\frac{Z_x}{Z_g}, \tag{8}$$

where $\varepsilon_{ye}=\varepsilon_{yr}\varepsilon_0$, $\mu_{xe}=\mu_{xr}\mu_0$, and $\mu_{ze}=\mu_{zr}\mu_0$. We further assume

$$\varepsilon_{ye} = -j\left(\frac{1}{\omega d}\right)\frac{1}{Z_g}, \quad \mu_{xe} = -j\left(\frac{1}{\omega d}\right)Z_z, \quad \mu_{ze} = -j\left(\frac{1}{\omega d}\right)Z_x. \tag{9}$$

When the unit cell is composed with series inductance $L_r/2$ in both x and z direction and shunting capacitance C_{gr} to ground, the *L-C* network becomes the ideal case of a 2D transmission line network, which represents conventional isotropic RHM with equivalent permittivity ε_{eRHM} and permeability μ_{eRHM} determined by shunted capacitance and series inductance per unit length, respectively. This can be directly derive from (9) to be

$$\varepsilon_{eRHM} = \frac{C_{gr}}{d}, \quad \mu_{eRHM} = \frac{L_r}{d}. \tag{10}$$

In the dual case, if the unit cell is composed with series capacitance $2C_l$ in both x and z direction and shunting inductance L_{gl} to ground, the *L-C* network becomes the ideal case of a 2D left-handed transmission line network, which can analogize isotropic LHM. The equivalent negative permittivity ε_{eLHM} and negative permeability μ_{eLHM} are determined by L_{gl} and C_l, and derive from (9) to be

$$\varepsilon_{eLHM} = -\frac{1}{\omega^2L_{gl}d}, \quad \mu_{eLHM} = -\frac{1}{\omega^2C_ld}. \tag{11}$$

Equations (10) and (11) are in consistent with the distributed *L-C* network equivalence of the normal dielectric media and LHM,[7,8] which reveals that the general equivalence of the constitutive parameters by Eq. (9) is reasonable.

In general case, the impedance elements Z_x, Z_z, and Z_g can be either capacitance or inductance, therefore, eight different types of the *L-C* networks can be constructed, as summarized in Table I. By choosing either capacitance or inductance as the impedance elements in the unit cell, we are able to construct different anisotropic *L-C* networks that can be used to realize all the four classes of media with different cutoff properties. For anisotropic unit cells with series capacitance in one direction and inductance in the other orthogonal direction, the *L-C* network can be used to realize AMMs with equivalent permeability having opposite sign in the two orthogonal directions. From Eq. (7) the dispersion relations of the anisotropic *L-C* networks become hyperbolic in the isofrequency plane, corresponding to either a *never-cutoff* or an *anti-cutoff* medium.

If the unit cell is composed with capacitance in both the series branches and shunting branch, the circuit becomes a capacitance network, which cannot support propagating wave and represent electromagnetic medium with positive permittivity and negative permeability, The dual case is converted to a inductance network, which also cannot support

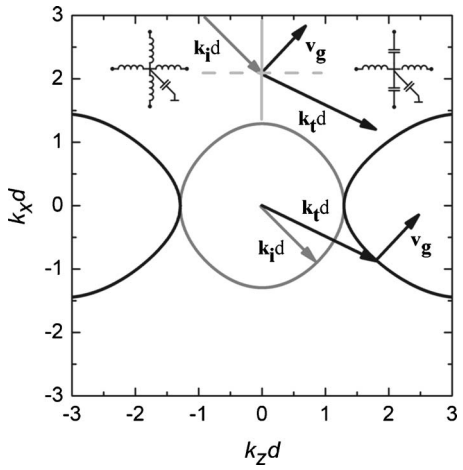

FIG. 2. Dispersion relations of the *L-C* circuits at 3.5 GHz representing isotropic RHM (gray line) and *never-cutoff* medium (black line) with unit cell shown in the upper left and right of the figure, respectively. The incident wave vector $\mathbf{k}_i$, refracted wave vector $\mathbf{k}_t$, and group velocity vector $\mathbf{v}_g$ are shown in the dispersion plot and in the refraction diagram.

propagating wave and represent electromagnetic medium with negative permittivity and positive permeability.[20]

The periodic *L-C* networks form a complete set of equivalent circuits which can realize electromagnetic media including isotropic or anisotropic RHM, isotropic or anisotropic LHM, and different AMMs. We can use the proposed equivalent circuits to study and realize both isotropic and anisotropic media, as well as interfaces of different metamaterials. This periodic circuit approach of both isotropic and anisotropic media is broadband with lower loss compared with other metamaterial approaches utilizing resonant unit cell elements. The effective constitutive parameters are obtained by choosing different types and values of the impedance elements which are arbitrary and easy to realize.

IV. ANALYSIS AND SIMULATION RESULTS

Isotropic *L-C* networks and its transmission line implantations have been used to study and realize electromagnetic wave propagation in isotropic RHM and LHM.[7–13] In this section, to verify the *L-C* network models of AMMs, we focus on using *L-C* networks to study electromagnetic wave propagation in the *never-cutoff* or *anti-cutoff* media.

A. *never-cutoff* medium

In Sec. III, we show that two types of anisotropic *L-C* network represent *never-cutoff* media. For example, it can be composed by *L-C* circuit with unit cell depicted in the upper right corner of Fig. 2. The network is serially connected by capacitor $2C_x$ in x direction and inductor $L_z/2$ in z direction, and shunted by capacitor C_g to ground. Under this assignment, $Z_x=1/j\omega C_x$, $Z_z=j\omega L_z$, and $Z_g=1/j\omega C_g$, and the dispersion relation (6) is reduced to

$$\cos k_x d - \frac{\omega_C^2}{\omega^2}\cos k_z d = \left(\frac{C_g}{2C_x}+1\right) - \frac{\omega_C^2}{\omega^2}, \tag{12}$$

where $\omega_C{}^2=1/C_xL_z$. When $k_xd \ll 1$, $k_zd \ll 1$, it is simplified to

$$-C_x\frac{(k_x d)^2}{C_g} + C_x\left(\frac{\omega_C^2}{\omega^2}\right)\frac{(k_z d)^2}{C_g} = 1, \tag{13}$$

which corresponds to hyperbolic curves in the isofrequency plane with the principle axis along the z axis. To study the electromagnetic wave propagation through the interface between isotropic RHM and the *never-cutoff* media, *L-C* network realization of the isotropic RHM is used with unit cell depicted in the upper left corner of Fig. 2. It is composed of serially connected inductors L_r in both x and z directions and shunting capacitor C_{gr}. The dispersion relation is

$$\cos k_x d + \cos k_z d = 2 - \frac{1}{2}\omega^2 L_r C_{gr}. \tag{14}$$

When $k_xd \ll 1$, $k_zd \ll 1$, it is simplified to

$$(k_x d)^2 + (k_z d)^2 = \omega^2 L_r C_{gr}, \tag{15}$$

which corresponds to circular curve in the isofrequency plane representing isotropic RHM. Figure 2 shows the dispersion relations for the two types of *L-C* networks in the isofrequency plane at 3.5 GHz with $C_x=0.5$ pF, $L_z=L_r=6$ nH, and $C_g=C_{gr}=0.5$ pF. Although the continuous medium approximation is not fully satisfied, the *L-C* network representing isotropic RHM or *never-cutoff* media has a dispersion curve very close to a circular curve or a hyperbolic curve, respectively.

Assuming a plane wave with electric field polarized in the y direction is incident on an interface between an isotropic RHM and a *never-cutoff* medium parallel to *x-y* plane. The two media are realized by *L-C* networks with circuit unit cells described in Fig. 2. The incident and refracted wave vector in the two media is depicted in Fig. 2 as $\mathbf{k}_i$ and $\mathbf{k}_t$ respectively, with the transverse component of the wave vector, $\mathbf{k}_x$, is conserved across the interface according to the boundary condition. The direction of energy propagation within the AMM can be found by calculating the group velocity, $\mathbf{v}_g=\nabla_k\omega(\mathbf{k})$,[17] which is not necessarily parallel to the wave vector and must lie normal to the isofrequency contour of the dispersion curves as shown in Fig. 2. Causality is considered to determine the correct direction of $\mathbf{v}_g$, which requires that the energy should propagate away from the interface in the *never-cutoff* medium. Therefore, the wave vector, or the phase velocity, undergoes positive refraction, while the energy propagation or the group velocity undergoes negative refraction.

To realize wave propagation through interface between an isotropic RHM and a *never-cutoff* medium, we construct a 2D *L-C* network composed with two periodic circuits with unit cells representing isotropic RHM and *never-cutoff* medium as schematically shown in Fig. 3. A linear interface between the two media is formed along the x direction and the network is extended in x and z directions with finite numbers of unit cells and resistively terminated to ground at the edges. A RF voltage source is placed in the upper left corner as an incident wave. The voltage distribution at each circuit node is explored using Agilent's Advanced Design System (ADS) microwave circuit simulator, which represents the electric field propagation in the media. Due to the weak

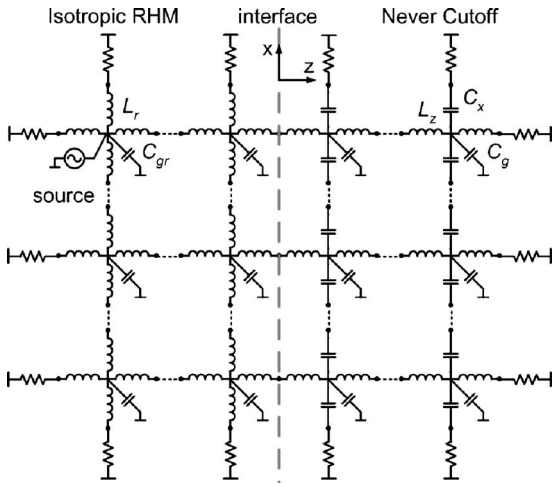

FIG. 3. Schematic of the *L-C* circuit network that represents interface of an isotropic RHM and a *never-cutoff* medium.

specular reflection from the edges, the node voltage spreading from the point source is mainly concentrated along the direction with 45° to the z direction, which results oblique incident wave to the interface with maximum power distributed at incident angle of 45°.

Figure 4 shows the magnitude and the phase distribution of the node voltages in the circuit at 3.5 GHz. The circuit has 25 unit cells along x direction and 50 unit cells along the z direction with the interface located between the 25th and 26th columns. Negative refraction of energy flow or the group velocity is observed in the magnitude distribution [Fig. 4(a)], while positive refraction of wave vector or phase velocity is observed in the phase distribution [Fig. 4(b)]. The refracted wave has a maximum power distribution mainly along the direction with a refraction angle of about −45°.

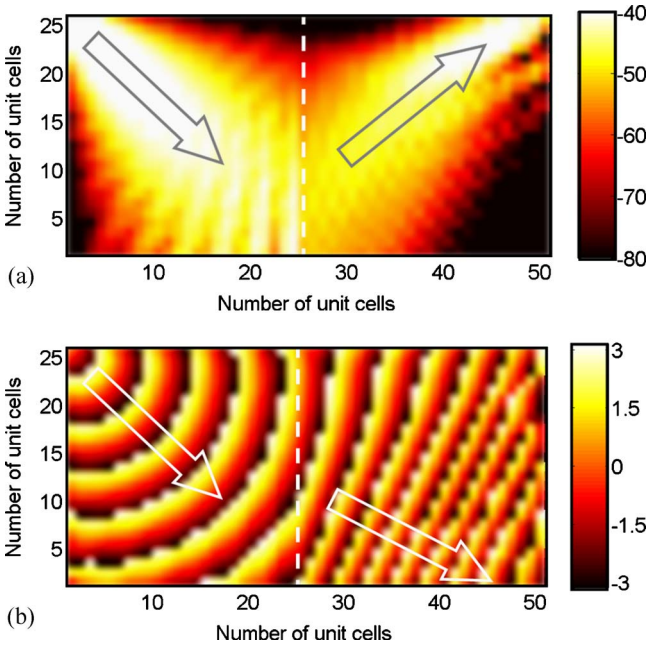

FIG. 4. (Color online) (a) Voltage magnitude (in dB) and (b) phase (in radian) distributions in the *L-C* circuit that represents a point source at the upper left corner illuminating the interface (dashed line) between an isotropic RHM and a *never-cutoff* medium at 3.5 GHz.

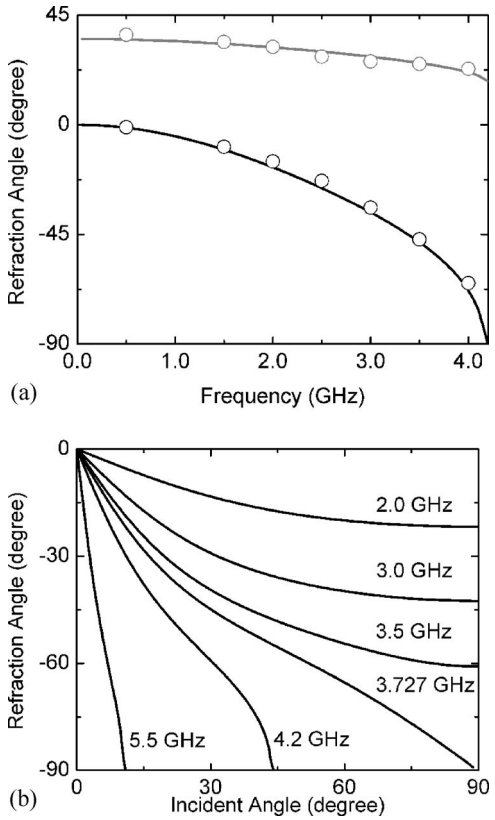

FIG. 5. (a) The theoretical calculations (lines) from Eqs. (16) and (17) and the ADS simulation results (circles) of the refraction angles of phase (gray) and energy flow (black) at different frequencies when a 45° incident wave propagates through the interface between isotropic RHM and *never-cutoff* medium. (b) Refraction angle of energy flow as a function of the incident angle at different frequencies.

The angle relation between the refracted wave vector $\mathbf{k}_t$ and the incident wave vector $\mathbf{k}_i$ is dominated by the dispersion equations (12) and (14) of the two media and the conservation of transverse component of the wave vector $\mathbf{k}_x$ across the interface. The direction of energy flow or the group velocity is obtained by $\mathbf{v}_g = \nabla_k \omega(\mathbf{k})$ in the *never-cutoff* medium. Therefore, we have

$$\theta_t^P = \tan^{-1}\frac{k_{tx}d}{k_{tz}d}, \tag{16}$$

$$\theta_t^G = \tan^{-1}\left[-\left(\frac{\omega}{\omega_C}\right)^2 \frac{\sin k_{tx}d}{\sin k_{tz}d}\right], \tag{17}$$

where θ_t^P, or θ_t^G is the refraction angle of phase or group velocity, respectively, and k_{tx}, or k_{tz} is the x or z component of the wave vector in the *never-cutoff* medium. Figure 5(a) shows the refraction angle of phase and group velocity calculated through Eqs. (16) and (17) at different operating frequencies for an incident angle of 45°. ADS simulations of the finite-sized circuit in Fig. 3 are also carried out at different

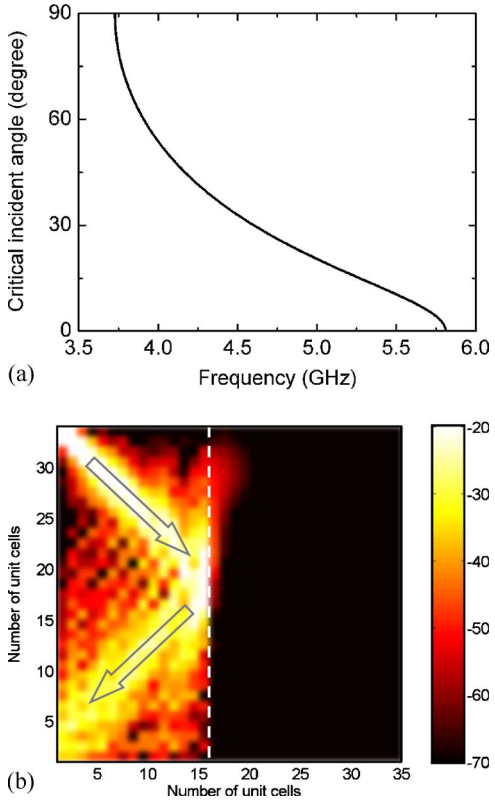

FIG. 6. (Color online) (a) Critical angles at different frequencies for waves propagating from isotropic RHM to *never-cutoff* medium represented by *L-C* circuits. (b) Voltage magnitude (in dB) distribution at 5.5 GHz in the *L-C* circuit that represents total reflection for a 45° incident wave at the interface (dashed line) between an isotropic RHM and a *never-cutoff* medium.

frequencies and the refraction angles θ_t^P, and θ_t^G are obtained from the phase and magnitude distribution of the node voltages and depicted in Fig. 5(a), which agree with the theoretical analysis from the infinite periodic circuit. Due to the dispersion, the 45° incident wave refracted at the interface with a negative angle of energy flow increasing from zero to 90°, together with a positive angle of wave vector decreasing from 35° to 18°, when the frequency increased from zero to 4.2 GHz. Further increasing the frequency, the 45° incident wave will be totally reflected. This can be demonstrated clearly in the relation between energy refraction angle and the incident angle in Fig. 5(b). At low frequency oblique incident wave is negatively refracted into the *never-cutoff* medium, but when the frequency exceeds a critical value of about 3.727 GHz, total reflection occurs for wave with incident angle exceeding the critical angle θ_i^C. Figure 6(a) shows the critical incident angle θ_i^C of total reflection which decreases with increasing the operating frequency. Figure 6(b) is the ADS simulation result for the circuit of Fig. 3 at 5.5 GHz. As the critical angle is about 10° at 5.5 GHz, the incident wave from the corner fed source with power distributed around 45° incident direction is almost totally reflected. Only a fraction of the incident wave with incident angle less than 10° refracts into the *never-cutoff* medium near the upper edge of the interface. Further increasing the frequency to the upper limit of 5.8 GHz, all *y*-polarized incident waves will be totally reflected.

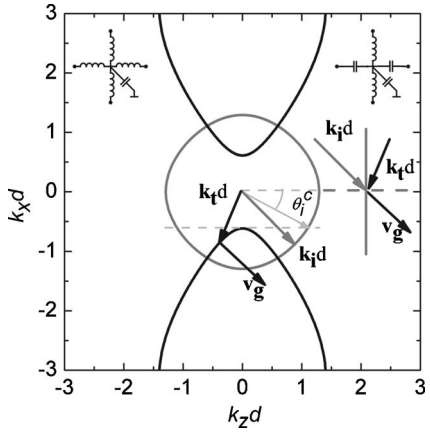

FIG. 7. Dispersion relations of the *L-C* circuits at 3.5 GHz representing isotropic RHM (gray line) and *anti-cutoff* medium (black line) with unit cells shown in the upper left and right of the figure, respectively. The incident wave vector $\mathbf{k}_i$, refracted wave vector $\mathbf{k}_t$ and group velocity vector $\mathbf{v}_g$ are shown in the dispersion plot and in the refraction diagram. The critical angle θ_i^c beyond which refraction occurs is also indicated in the figure.

B. *Anti-cutoff* medium

Now we consider the anisotropic *L-C* network that could realize the *anti-cutoff* medium. As shown in Sec. III, the *anti-cutoff* medium can be realized by two types of *L-C* circuits, for example, by *L-C* circuit with unit cell depicted in the upper right corner of Fig. 7. In the unit cells, $Z_x = j\omega L_x$, $Z_z = 1/j\omega C_z$, and $Z_g = 1/j\omega C_g$, and the dispersion relation (6) is reduced to

$$-\frac{\omega_C^2}{\omega^2}\cos k_x d + \cos k_z d = \left(\frac{C_g}{2C_z} + 1\right) - \frac{\omega_C^2}{\omega^2}, \tag{18}$$

where $\omega_C^2 = 1/C_z L_x$. When $k_x d \ll 1$, $k_z d \ll 1$, it is simplified to

$$C_z\left(\frac{\omega_C^2}{\omega^2}\right)\frac{(k_x d)^2}{C_g} - C_z\frac{(k_z d)^2}{C_g} = 1, \tag{19}$$

which corresponds to hyperbolic curves in the isofrequency plane with the principle axis along the *x* axis.

Consider the interface between isotropic RHM and *anti-cutoff* medium composed with two periodic circuits with unit cells depicted in the upper left and right corner of Fig. 7, respectively. The dispersion relation for the two *L-C* networks in the isofrequency plane is shown in Fig. 7 at 3.5 GHz with $C_z = 1.5$ pF, $L_x = 3$ nH, $C_g = 0.25$ pF, $L_r = 6$ nH, and $C_{gr} = 0.5$ pF. The *L-C* network representing *anti-cutoff* medium has a dispersion curve close to a hyperbolic one. When electromagnetic wave propagating from the isotropic RHM to the *anti-cutoff* medium, by matching the transverse component of the wave vector $\mathbf{k}_x$ across the interface according to the boundary condition, we find that the wave vector undergoes a negative refraction, while the energy flow or the group velocity undergoes positive refraction. The *z* components of the wave vectors are antiparallel in the two media indicating a backward wave characteristic along *z* direction in the *anti-cutoff* medium. This has been depicted in Fig. 7.

The refraction angles for the wave vector $\mathbf{k}_t$ and the en-

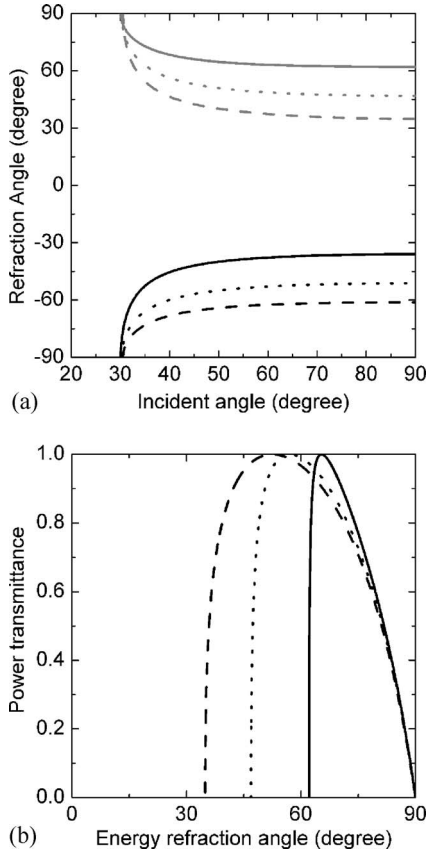

FIG. 8. (a) Refraction angles of phase (black) and energy flow (gray) for different incident angles, and (b) power transmittance for different energy refraction angles at 1.5 GHz (solid line), 2.5 GHz (dotted line), and 3.5 GHz (dashed line), respectively, for a plane wave propagation through the interface of an isotropic RHM and an *anti-cutoff* medium resembled by *L-C* networks shown in Fig. 7.

ergy flow or group velocity $\mathbf{v}_g$ in the *anti-cutoff* medium have been calculated from the dispersion equation (18) and shown in Fig. 8(a) at different frequencies. Total reflection occurs for normal incident wave or wave with small incident angles. As the incident angle increases, there exists a critical value for the incident angle θ_i^c determined by the dispersion relation (see Fig. 7), above which the wave begins to refract into the *anti-cutoff* medium. Such inversion of the critical angle is distinct from what happens at the interface of conventional dielectric media that the total reflection only occurs for wave with incident angle larger than a critical angle. Such anomalous phenomenon is caused by the dispersion relation in the *anti-cutoff* medium which leads to a decreasing function of the incident angle for both the energy and the phase refraction angles. When increasing the frequency the phase refracts at a larger negative angle, while the energy refracts at a smaller positive angle.

When a plane wave impinging on the interface of an isotropic RHM and an *anti-cutoff* medium, the Fresnel formula for the reflectance Γ can be derived by applying the conservation of parallel components of E and H at the interface, which is

$$\Gamma = \frac{\cos\theta_i - \sqrt{\frac{\varepsilon_y\mu_1}{\varepsilon_1\mu_x} - \frac{\mu_1^2}{\mu_x\mu_z}\sin^2\theta_i}}{\cos\theta_i + \sqrt{\frac{\varepsilon_y\mu_1}{\varepsilon_1\mu_x} - \frac{\mu_1^2}{\mu_x\mu_z}\sin^2\theta_i}}, \tag{20}$$

where θ_i is the incident angle and ε_1, μ_1 are the permittivity and permeability of the isotropic RHM, respectively.[21] The effective constitutive parameters of the *anti-cutoff L-C* circuit network can be calculated by impedances of the circuit elements through Eq. (9). At small incident angle θ_i, the value in the square root of Eq. (20) is negative, yielding a reflectance of $|\Gamma|=1$. The critical angle θ_i^c is determined when the square root of Eq. (20) is zero, which yields $\theta_i^C = \sin^{-1}\sqrt{\varepsilon_y\mu_z/\varepsilon_1\mu_1}$. For *anti-cutoff L-C* network shown in Fig. 7, $\theta_i^C = \sin^{-1}\sqrt{C_gL_x/C_{gr}L_r} = 30°$, according with the results in Fig. 8(a). The electromagnetic power transmittance can be calculated by

$$T_S = \frac{S_t}{S_i} = 1 - |\Gamma|^2, \tag{21}$$

and shown in Fig. 8(b) at different frequencies, where S_t and S_i are the values of the incident and the transmitted Poynting vector, respectively. When the wave impinging at an angle exceeding the critical angle θ_i^c, it begin to refract and the transmittance increases rapidly to 1, where total transmission takes place, and then decreases leading to strong reflection again. The total transmission obtained here is different from the Brewster effect at the interface of conventional isotropic media which describes the zero reflectivity of a *P*-polarized wave (**H** parallel to *y* axis) at an incidence angle satisfying $\theta_i + \theta_t = \pi/2$.[21] This anomalous Brewster effect in the *anti-cutoff* medium is a consequence of the anisotropy in a dispersive media, which makes it transparent to an oblique incident wave at a particular angle and dark to other incident wave.[18]

To verify the anomalous reflection and transmission phenomenon at the interface of an isotropic RHM and an *anti-cutoff* medium realized by *L-C* circuit networks, we construct a 2D *L-C* network similar to Fig. 3 using the unit cells depicted in Fig. 7 representing isotropic RHM and *anti-cutoff* medium. The interface is located between the 15th and the 16th columns and a RF voltage source is applied in the center of the isotropic RHM at the node of the 8th column with the 25th row (black point in Fig. 9). The point source irradiates electromagnetic wave to the interface with incident angle ranges from zero to 74° at the two ends of the interface. Figure 9(a) shows the ADS circuit simulation results of the node voltage distribution at 3.5 GHz, which represents the electric field propagation through the interface of an isotropic RHM and an *anti-cutoff* medium. As expected, wave impinging at a small angle including normal incident is totally reflected, and the refracted power in the *anti-cutoff* medium is concentrated along direction with an angle around 50°, which corroborate the theoretical prediction that the Brewster angle at 3.5 GHz is about 52° as shown in Fig. 8(b).

When changing the parameters of the circuit for the *anti-cutoff* medium so that $\sin\theta_i^C = (\varepsilon_y\mu_z/\varepsilon_1\mu_1)^{1/2} > 1$, the disper-

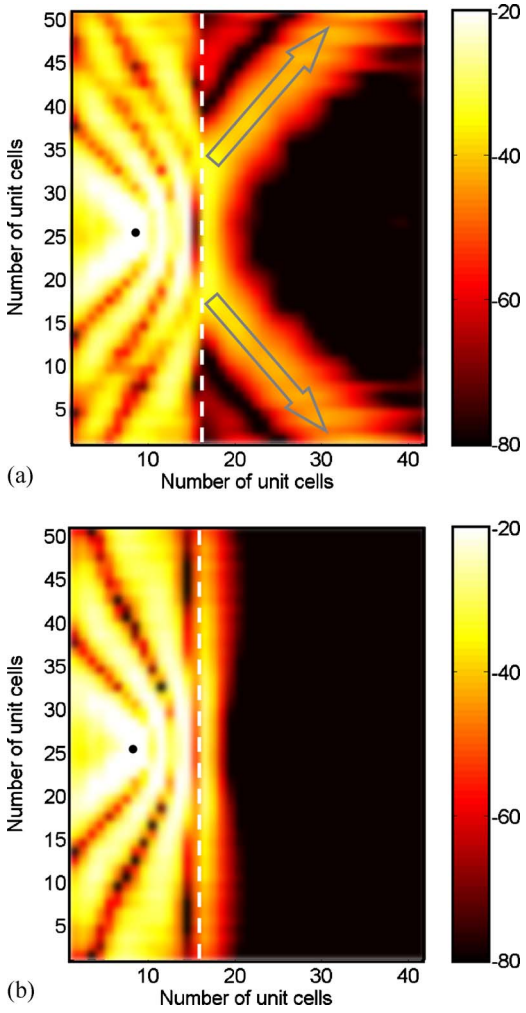

FIG. 9. (Color online) Voltage magnitude (in dB) distribution at 3.5 GHz in the *L-C* circuit that represents a point source (depicted by the black point) illuminating the interface (dashed line) between an isotropic RHM and an *anti-cutoff* medium. (a) Transmission at particular oblique angle, (b) total reflection as the circuit parameters change to C_z=0.5 pF, L_x=6.6 nH, and C_g=0.55 pF.

sion curves of the isotropic RHM and the *anti-cutoff* medium cannot cross with each other and the phase matching condition cannot be satisfied on the hyperbola, indicating that any incident wave is totally reflected at the interface. This is illustrated in Fig. 9(b) by ADS simulation on the circuit with changed unit cell parameters of the *anti-cutoff* medium. All the waves irradiated from the point source are totally reflected at the interface, while only evanescent fields propagate in the *anti-cutoff* medium that decay exponentially away from the interface.

C. Implementation of AMM by transmission line network

From the above sections, we have verified the validity of *L-C* network circuit models for different kind of AMMs through both the periodic circuit analysis of the infinite 2D array with unit cell described in Table I, and the microwave circuit simulations of the wave propagation in circuit network of finite size. The *L-C* circuit models of AMMs not only give more physical insight into the anomalous wave propagation in such AMMs, but also could lead to new approach of actual implementation of different kind of AMMs. In the following we will show example that actual realization of one of the AMMs, the *never-cutoff* media, could be possible based on the *L-C* circuit models.

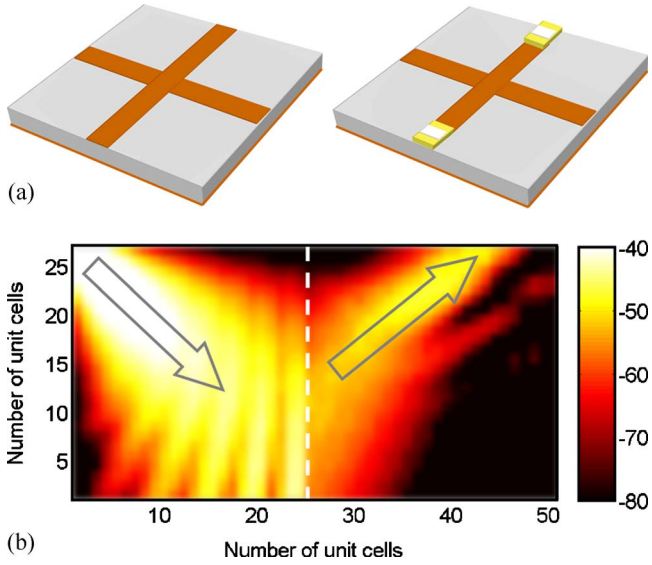

FIG. 10. (Color online) (a) Schematic of the unit cells of TL based metamaterials. Left is for the microstrip line grid to realize isotropic RHM, and the right is for the microstrip line grid loaded with series chip capacitances in one orthogonal direction to realize the *never-cutoff* medium. (b) Voltage magnitude (in dB) distribution in the 2D TL metamaterial that represents a point source at the upper left corner illuminating the interface (dashed line) between an isotropic RHM and a *never-cutoff* medium at 3.5 GHz.

The TL versions of isotropic RHM and LHM have been investigated by Eleftheriades *et al.*[7] and Caloz *et al.*[9] based on the *L-C* circuit model of RHM and LHM. From the electromagnetic theory, lossless TL can be modeled as periodic network of series per-unit-length inductance and shunt per-unit-length capacitance, therefore an isotropic RHM could be realized by 2D periodic TL grid and an isotropic LHM could be realized by 2D periodic TL grid loaded with series capacitance and shunt inductance. Based on the *L-C* circuit models of the AMMs described in Table I, it is straight forwards that 2D periodic TL grid loaded with series capacitance along one of the orthogonal directions could be used to realize the *never-cutoff* media or the *anti-cutoff* media.

To actually implement the AMMs through the TL based approach, we used microstrip line grid structure to synthesize 2D isotropic RHM and the *never-cutoff* medium. The microstrip is designed with a characteristic impedance of 70 Ω with copper strip on a grounded microwave substrate of thickness of 1.5 mm, dielectric constant ε_r=4.0 and loss tangent of 2×10^{-3}, which could be easily fabricated by printed circuit-board technique. Similar to the circuit in Fig. 3, we construct an interface between isotropic RHM and *never-cutoff* medium. The isotropic RHM is composed of 25×25 unit cells of the microstrip line grid as shown in the left of Fig. 10(a), while the *never-cutoff* medium is composed of 25×25 unit cells of the microstrip line grid loaded by series chip capaci-

tance along the direction parallel to the interface as shown in the right of Fig. 10(a). In the design, we use 1 pF chip capacitance from the AVX Company (AQ 11). The microstrip circuit is designed to have similar equivalent constitutive parameters to that of the circuit in Fig. 3 and each unit cell has a dimension of about 5×5 mm^2. The detailed designing of the AMMs through TL metamaterial will be reported separately.

To study the negative refraction at the interface, we place a RF voltage source in the upper left corner as an incident wave. The voltage distribution of the microstrip circuit is simulated by ADS simulator. In the simulation we have included both the microstrip line loss (metallic loss and the dielectric loss) and the loss associated with the chip capacitance. Figure 10(b) shows the simulated results at 3.5 GHz, which demonstrated the negative refraction of energy flow at the interface between isotropic RHM and *never-cutoff* medium. Comparing with Fig. 4(a), the voltage distribution show similar refraction angle of the energy flow but about 10 dB less of the magnitude of the maximum voltage due to the inclusion of the losses in the simulation. Therefore, the losses in the TL metamaterials affect only the magnitude of the propagating energy, not the refraction phenomenon.

V. CONCLUSIONS

In conclusion, we have proposed a complete set of periodic *L-C* circuit networks which can realize electromagnetic wave propagation in 2D media including both isotropic and anisotropic metamaterials. The 2D periodic circuit is constructed with unit cell of series capacitance or inductance in orthogonal directions, together with either capacitance or inductance shunted to ground. The dispersion relations of the periodic circuits could be either elliptic or hyperbolic in phase space depending on the types of the impedance elements in the unit cells. We have particularly shown that anisotropic *L-C* circuits could exhibit the wave propagation characteristics of either *never-cutoff* or *anti-cutoff* medium. We have constructed interfaces of isotropic RHM and AMMs with properly designed isotropic and anisotropic *L-C* circuits and analyzed the electromagnetic wave propagation using ADS microwave circuit simulations. We have demonstrated anomalous electromagnetic wave reflection and refraction phenomena at the interfaces that have good agreements with the theoretical analysis. Furthermore, we show that the *L-C* circuit models of AMMs could lead to different approach of actual implementation of 2D AMMs through TL based metamaterials. We have given example of designing *never-cutoff* medium by periodic microstrip line grid loaded with series chip capacitance along one orthogonal direction. The simulation on the actual structure reveals that similar wave propagation phenomenon could be obtained, and the losses in the TL metamaterial only affect the magnitude of the propagating energy. The circuit representation of both isotropic and anisotropic media is broadband with low loss, and easy to realize with arbitrary effective constitutive parameters. We believe the proposed *L-C* circuit network models provide not only alternative method to study the anomalous wave propagation in the AMMs, but also TL implementations of interesting planar RF/microwave devices that could utilize the extraordinary phenomena of both the isotropic and anisotropic metamaterials.

ACKNOWLEDGMENTS

This work is supported by the National Basic Research Program of China (under project 2004CB719800), the Specialized Research Fund for the Doctoral Program of Higher Education (No. 20030284024), and partially supported by the National Nature Science Foundation (No. 40401046).

*Electronic address: yjfeng@nju.edu.cn

[1] J. B. Pendry, A. J. Holden, D. J. Robbins, and W. J. Stewart, IEEE Trans. Microwave Theory Tech. **47**, 2075 (1999).
[2] J. B. Pendry, Phys. Rev. Lett. **85**, 3966 (2000).
[3] D. R. Smith, W. J. Padilla, D. C. Vier, S. C. Nemat-Nasser, and S. Schultz, Phys. Rev. Lett. **84**, 4184 (2000).
[4] R. A. Shelby, D. R. Smith, S. C. Nemat-Nasser, and S. Schultz, Appl. Phys. Lett. **78**, 489 (2001).
[5] A. A. Houck, J. B. Brock, and I. L. Chuang, Phys. Rev. Lett. **90**, 137401 (2003).
[6] C. G. Parazzoli, R. B. Greegor, K. Li, B. E. C. Koltenbah, and M. Tanielian, Phys. Rev. Lett. **90**, 107401 (2003).
[7] G. V. Eleftheriades, A. K. Iyer, and P. C. Kremer, IEEE Trans. Microwave Theory Tech. **50**, 2702 (2002).
[8] A. K. Iyer and G. V. Eleftheriades, in *IEEE MTT-S Int. Microwave Symp. Dig.* (IEEE Inc., Seattle, WA, 2002), Vol. 2, p. 1067.
[9] C. Caloz, H. Okabe, T. Iwai, and T. Itoh, in *Proceeding of USNC/URSI National Radio Science Meeting* (USNC/URSI, San Antonio, TX, 2002), p. 39.
[10] A. Grbic and G. V. Eleftheriades, Appl. Phys. Lett. **82**, 1815 (2003).
[11] A. Grbic and G. V. Eleftheriades, IEEE Trans. Antennas Propag. **51**, 2604 (2003).
[12] A. Grbic and G. V. Eleftheriades, Phys. Rev. Lett. **92**, 117403 (2004).
[13] C. Caloz and T. Itoh, IEEE Trans. Antennas Propag. **52**, 1159 (2004).
[14] R. Shelby, D. R. Smith, and S. Schultz, Science **292**, 77 (2001).
[15] A. N. Lagarkov and V. N. Kissel, Phys. Rev. Lett. **92**, 077401 (2004).
[16] V. Lindell, S. A. Tretyakov, K. I. Nikoskinen, and S. Ilvonen, Microwave Opt. Technol. Lett. **31**, 129 (2001).
[17] D. R. Smith and D. Schurig, Phys. Rev. Lett. **90**, 077405 (2003).
[18] Lei Zhou, C. T. Chan and P. Sheng, Phys. Rev. B **68**, 115424 (2003).
[19] D. R. Smith, D. Schurig, J. J. Mock, P. Kolinko, and P. Rye, Appl. Phys. Lett. **84**, 2244 (2004).
[20] A. Alù and N. Engheta, IEEE Trans. Antennas Propag. **51**, 2558 (2003).
[21] J. A. Kong, *Electromagnetic Wave Theory* (EMW, Cambridge, MA, 2000).